Parameter-space topology of models for cell polarity

Parameter-space topology of models for cell polarity

Philipp Khuc Trong[1,2,7]**, Ernesto M Nicola**[3]**, Nathan W Goehring**[4,5]**, K Vijay Kumar**[1,2,6] **and Stephan W Grill**[1,2,6]

[1] Max-Planck Institute for the Physics of Complex Systems, Nöthnitzer Straße 38, D-01187 Dresden, Germany
[2] Max-Planck Institute of Molecular Cell Biology and Genetics, Pfotenhauer Straße 108, D-01307 Dresden, Germany
[3] IFISC, Institute for Cross-Disciplinary Physics and Complex Systems (CSIC-UIB), Campus Universitat Illes Balears, Palma de Mallorca, Spain
[4] CRUK London Research Institute, Lincoln's Inn Fields Laboratories, 44 Lincoln's Inn Fields, London WC2A 3LY, UK
[5] MRC-LMCB, University College London, Gower Street, London WC1E 6BT, UK
[6] BIOTEC, Technische Universität Dresden, Tatzberg 47/49, D-01307 Dresden, Germany
E-mail: stephan.grill@biotec.tu-dresden.de

Abstract

Reaction–diffusion systems have been widely successful in the theoretical description of biological patterning phenomena, giving rise to numerous models based on differing mechanisms, mathematical implementations and parameter choices. However, even for models with common design features, the diversity of mathematical realizations may hinder the identification of common behavior. Here, we analyze three different reaction–diffusion models for cell polarity that feature conservation of mass, rapid cytoplasmic diffusion and bistability via a cusp bifurcation of uniform states. In all three models, the nonuniform polar states are front solutions, and growth of domains ceases through stalling of a propagating front. For these three models we find a characteristic parameter space topology, comprising a region of linear instability that loops around the cusp point and that is enclosed by a 'comet-shaped' region of nonuniform domain states. We propose a minimal model based on the cusp bifurcation normal form that includes essential characteristics of all cell polarity models

[7] Present address: Department of Applied Mathematics and Theoretical Physics, Centre for Mathematical Sciences, University of Cambridge, Wilberforce Road, CB3 0WA, UK.

considered. For this minimal model, we provide a complete analytical description of the parameter space topology, and find that the instability loop appears as a generic property of the cusp bifurcation. This topological analysis provides a unifying understanding of earlier mathematically distinct models and is suitable to classify future models.

Keywords: cell polarity, reaction-diffusion equations, cusp bifurcation

The emergence of patterns in biology has long raised the interest of theorists attempting to explain the underlying mechanisms. Cell polarity is typically defined as an asymmetric distribution of signaling molecules, often associated with the cell membrane. It occurs in many cell types and is fundamental to processes as diverse as cell motility, differentiation and asymmetric cell divisions [1].

While polarization in different cell types can differ in the number and identity of interacting protein species, the type of interactions, and the mechanisms that trigger polarization, global features are often similar. For example, polarity proteins are often associated with the cell membrane but can also enter the cytoplasm. Generally, these membrane-associated systems are accompanied by no or very weak cytoplasmic gradients. This suggests a much higher mobility for proteins in the bulk cytoplasm compared to the mobility when associated to the membrane, leading to a separation of time scales. Furthermore, cell polarization often occurs on time scales of minutes on which degradation or de-novo production of proteins is negligible, thereby establishing an approximately conserved total amount of signaling proteins inside the cell [2–6].

Several previously proposed theoretical models for cell polarization feature both strongly diverging diffusion constants between cytoplasmic and membrane-bound states as well as conservation of total protein amount. Based on known biochemistry and in some cases on biophysical experiments, these models capture observations of cell polarity in chemotaxis [2–4, 7] and asymmetric cell divisions [5, 6]. Some of these studies were also accompanied by simplified, conceptual models in an attempt to deduce the essential ingredients [3, 4, 7]. Moreover, under certain conditions of the chemical reaction kinetics, the evolving patterns are propagating fronts that stall via the depletion of cytoplasmic protein supply [8, 9].

Three questions arise from this. First, beyond either highlighting abstract design principles or model behaviors at individual parameter values, what is a feasible way to comprehensively, yet compactly, characterize the behavior of a given model even for larger variations of parameters? Second, how does a comprehensive characterization of one model compare to other models? In particular, do common design principles such as rapid cytoplasmic diffusion, conservation of total protein amount and a front-stalling mechanism translate into an exactly equivalent common repertoire of possible behaviors despite vastly different implementation of chemical kinetics? Third, if there exists a family of models according to the above two criteria, can a simple and representative minimal model offer new insights into the origin of the underlying similarities?

Here we answer these questions by portraying a family of three models for cortical cell polarity that are based on mass-conservation, rapid cytoplasmic diffusion, and bistability of uniform states by a cusp bifurcation but differ in the number of interacting chemical species as well as in the kinetic functions that govern their interaction. First, we recapitulate and expand

the characterization of a single model for PAR protein polarity by investigating the makeup of uniform states, their linear stability properties as well as the existence and distribution of nonuniform states in parameter space. Second, we show that the same parameter space topology found in the first model also characterizes two previously published models, thereby implying an unexpected common repertoire of possible behaviors, despite strong differences in their mathematical realization. Third, we define a minimal model based on the cusp bifurcation normal form and derive analytical expressions for all topological structures. Our analysis of the minimal model suggests further that the characteristic shape of the regime of linear instability is a fundamental property of the cusp bifurcation.

Thus, the topology identified in this work appears as a suitable way to classify future models of cell polarity, and to understand and communicate behavior and robustness associated with a specific choice of parameters.

1. Common features of cell polarity models

We begin our analysis by highlighting the general features of the reaction–diffusion models considered here. All models describe one or several chemical species i that can cycle between a cytoplasmic state with concentration v_i and a membrane bound state with concentration u_i. The only chemical reactions that occur are interconversions of protein between these two states that conserve the total amount of each protein species individually. All models are considered on a one dimensional (1D) line with spatial and temporal coordinates x and t. The system of equations are of the form

$$\frac{\partial u_i}{\partial t} = D_{u,i}\frac{\partial^2 u_i}{\partial x^2} + f_i\left(u_1,...,u_N, v_1,...,v_N\right) \tag{1}$$

$$\frac{\partial v_i}{\partial t} = D_{v,i}\frac{\partial^2 v_i}{\partial x^2} - f_i\left(u_1,...,u_N, v_1,...,v_N\right) \tag{2}$$

$$\rho_{0,i} = \frac{1}{L}\int_0^L \mathrm{d}x\left[u_i(x, t) + v_i(x, t)\right], \tag{3}$$

where $D_{u,i}$ and $D_{v,i}$ represent the respective diffusivities in the cortical and cytoplasmic compartments. f_i denote the reaction terms that can in general depend on all N protein species. The total concentration of each species can be calculated according to equation (3), which is an additional parameter of the system set by the initial condition. We consider all systems in the limit of rapid cytoplasmic diffusion $D_{u,i} \ll D_{v,i}$. In this case, the cytoplasmic concentrations are essentially constant throughout space $v_i(x, t) = v_i(t)$. Importantly, the conservation law (3) can be used to compute the uniform cytoplasmic concentrations from the cortical concentrations alone $v_i(t) = \rho_{0,i} - 1/L\int u_i(x, t)\mathrm{d}x$. Substituting $v_i(t)$ in (1) then reduces the system of $2N$ differential equations to a system of N integro-differential equations

$$\frac{\partial u_i}{\partial t} = D_{u,i}\frac{\partial^2 u_i}{\partial x^2} + f_i\left(u_1,...,u_N, \left\langle u_1\right\rangle,...,\left\langle u_N\right\rangle\right), \tag{4}$$

wherein $\left\langle u_i\right\rangle(t)=1/L\int u_i(x, t)\,\mathrm{d}x$ denotes the global average. Through this reduction, the N mass constraints are included explicitly in the equations.

In the following sections, we analyze several reaction–diffusion models with differing choices of kinetic functions f_i with respect to their uniform states, their stability properties and the coexistence of polar nonuniform states. The combination of uniform states, stability properties and presence or absence of a polar nonuniform state is collectively referred to as the behavior of the given model at the chosen point in parameter space. The parameter space topology of a given model denotes the entirety of model behaviors found for variation of the control parameters within the range shown. Hence, two models that share a common parameter space topology also share a common repertoire of behaviors.

Simulations of nonuniform concentration profiles were performed using a finite-difference discretization method with Runge–Kutta 4th order integration scheme and fixed time step Δt implemented in custom C++ code. The bistability regions were calculated using either Matcont version 2.5.1 [10] or custom C++ code. Mathematica 7 [11] as well as custom C++ code were employed to compute the outline of the instability loops.

2. Models of cell polarity

2.1. The PAR protein model

We recently proposed a reaction–diffusion model in the form of (4) to describe the polarization of PAR proteins during the first asymmetric cell division in the roundworm *C. elegans* [6]. For two protein species aPAR (the anterior PAR complex, $i \equiv A$) and pPAR (the posterior PAR complex, $i \equiv P$), the kinetic functions were defined as

$$f_P\left(u_A,\, u_P,\, \langle u_P \rangle\right) \;=\; k_{\mathrm{on},P}\left(\rho_{0,P} - \Psi \langle u_P \rangle\right) - k_{\mathrm{off},P}u_P - k_{PA}u_P u_A^{\alpha},$$

$$f_A\left(u_A,\, u_P,\, \langle u_A \rangle\right) \;=\; k_{\mathrm{on},A}\left(\rho_{0,A} - \Psi \langle u_A \rangle\right) - k_{\mathrm{off},A}u_A - k_{AP}u_A u_P^{\beta}, \tag{5}$$

wherein Ψ denotes a surface-to-volume conversion factor and α and β are stochiometric coefficients [6]. In addition to membrane association and dissociation, with respective rate constants k_{on} and k_{off}, the chemical reactions in this model involve mutually antagonistic interactions of protein complexes in their active state on the membrane represented by the membrane dissociation terms $k_{PA}u_P u_A^{\alpha}$ and $k_{AP}u_A u_P^{\beta}$.

To highlight the general properties of this model, we analyze its behavior for a symmetric parameter set in which the respective parameters of the two species are identical. For the k_{PA}-k_{AP} parameter space (figure 1) we use the following set of parameters: $D_A = D_P = 1\mu\mathrm{m}^2\mathrm{s}^{-1}$, $k_{\mathrm{off},A} = k_{\mathrm{off},P} = 0.3\mathrm{s}^{-1}$, $k_{\mathrm{on},A} = k_{\mathrm{on},P} = 1\mu\mathrm{ms}^{-1}$, $\rho_{0,P} = \rho_{0,A} = 1\mu\mathrm{m}^{-3}$, $\alpha = \beta = 2$ and $\Psi = 0.3\mu\mathrm{m}^{-1}$. For the $\rho_{0,P}$-$\rho_{0,A}$ parameter space (figure 2(A)) we use the same parameter set except that the values $k_{PA} = k_{AP} = 1\mu\mathrm{m}^4\,\mathrm{s}^{-1}$ are kept fixed. Simulations were performed with $\Delta t = 0.01\,\mathrm{s}$ for a system length $L = 100\,\mu\mathrm{m}$ with 200 grid points spaced $\Delta x = 0.5\,\mu\mathrm{m}$ apart and periodic boundary conditions.

In characterizing the behavior of this model as a function of the interaction rate constants k_{PA} and k_{AP}, we found a region of bistability of homogeneous steady-states (figure 1(A), (iii)) which culminates in a cusp bifurcation point. Furthermore, the system is capable of supporting inhomogeneous domain states (figure 1(C), green with dashed boundary) that resemble the final segregation of PAR proteins when polarization is complete. Note that, contrary to other
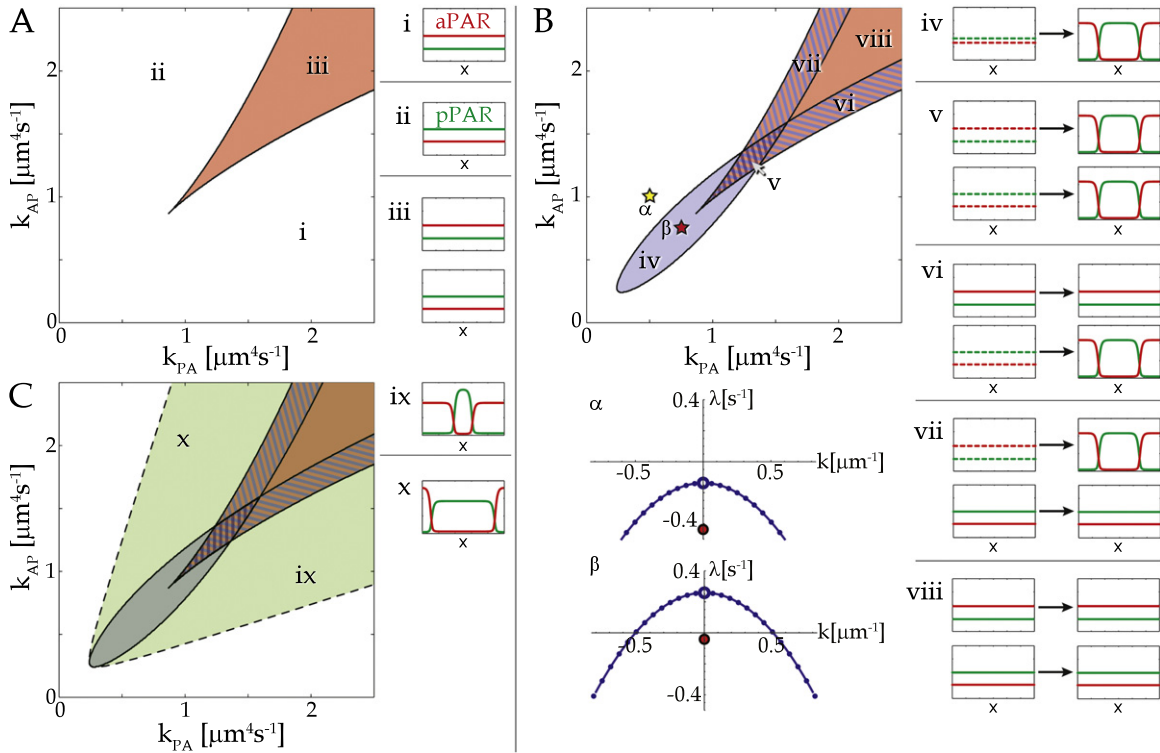
Figure 1. Successive construction of the parameter space topology exemplified by the model of PAR protein polarization in *C. elegans* (5) explored as function of the interaction rate constants k_{AP} and k_{PA}. (A) Outside the region of bistability only one uniform steady-state exists that can either be dominated by high aPAR (i) or high pPAR concentration. Inside the region of bistability (iii), both steady-states coexist and are stable with respect to uniform perturbations, separated by a third steady-state that is unstable (not shown). (B) In addition to the region of bistability of panel (A), the region of instability (iv)–(vii) is shown, indicating the areas in which nonuniform perturbations destabilize either all (iv), (v), exactly one (vi), (vii) or none of the homogeneously stable uniform states (viii). Cartoons (iv)–(viii) visualize the response of each steady-state to small nonuniform perturbations (black arrows). Small perturbations either decay back to the stable steady-states (solid lines) or grow and form polarized patterns from unstable steady-states (dashed lines). (α) and (β) show the largest growth rate of the unique uniform steady-state at two parameter sets indicated in panel (B) (stars). Outside the instability loop the growth rate is negative and perturbations below a threshold are decaying (α), while inside the loop the system is unstable with the largest growth rate at $k_1 = 2\pi/L$ (β). (C) Shown are the same regions of bistability and instability as in panel (B). Additionally, the region of polar inhomogeneous states is overlaid (green, dashed boundary). Near the lower boundary the aPAR domain is wide (ix), while near the upper boundary the pPAR domain is wide (x).

approaches [8], the concentration values of the homogeneous steady-states here do not have a direct relation to the concentration values of the inhomogeneous patterns.

For a large fraction of parameter space, the transition between a homogeneous steady-state and the coexisting domain state depends on an external trigger to overcome a finite perturbation threshold. *In vivo*, such a trigger is provided by advective cortical flow [6], thereby coupling mechanical cues to biochemical pattern formation [12].
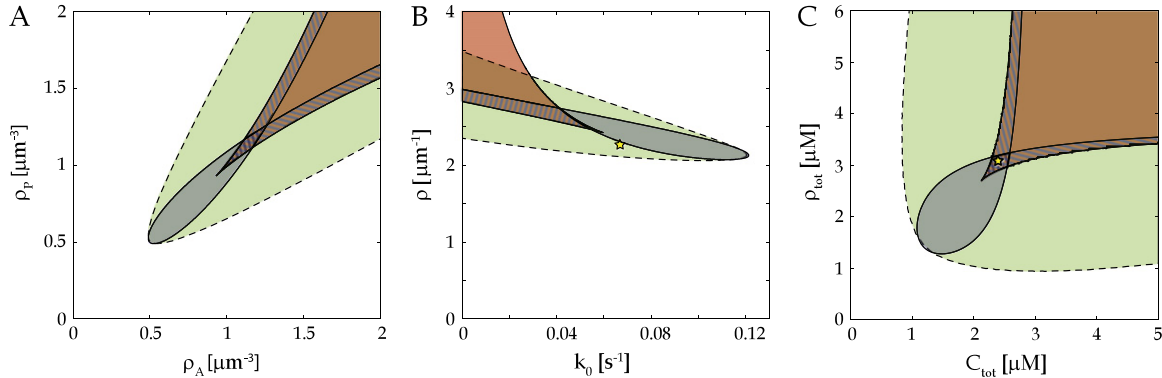
Figure 2. A common topology spans across diverse models for cortical cell polarity. (A) For variations of protein amounts ρ_P and ρ_A the PAR protein model [6] shows a region of bistability (orange) within a cusp bifurcation, a loop-shaped region of linear instability (blue, blue dashed) and a region of domains (green, dashed boundary) arranged in the same topology as for variations of the interaction rate constants (figure 1(C)). (B) The wave-pinning model [8] shows an identical topology as the PAR protein model despite featuring only one protein species and different kinetic functions. Color coding as in panel (A). Yellow star indicates parameter values chosen in [8]. Note, however, that the instability region shown here is slightly enlarged compared to the originally formulated system [8] due to the infinite cytoplasmic diffusion. (C) A model for polarization of small Rho-GTPases [2] again shows the same topology. Color coding as in panel (A). Star indicates parameters chosen in [2].

The transition between the homogeneous state and polarized state may also occur spontaneously. This would be the case when the perturbation threshold vanishes and the homogeneous states become linearly unstable, exhibiting a positive growth rate for some exponentially growing perturbation modes. To determine whether or not the PAR protein model (5) shows zero-threshold regimes, we performed a linear stability analysis to test the behavior of the uniform steady-states $X_0 = \left(A_0, P_0\right)^T$ under small perturbations. We use the ansatz $X = X_0 + \tilde{X}$ where the perturbation is $\tilde{X} = \eta \exp\left(\sigma t + ikx\right) + c.c$, with $c.c$ denoting the complex conjugate. Inserting this ansatz in equation (5) and linearizing, we obtain the eigenvalue equation $\sigma\left(k\right) \tilde{X} = \tilde{J}\left(k\right) \cdot \tilde{X}$ with the following form of the Jacobian in Fourier space:

$$\tilde{J} = -\begin{pmatrix} D_A k^2 + k_{\text{off},A} + \Psi k_{\text{on},A}\delta_{k,0} + k_{AP}P_0^{\alpha} & \alpha k_{AP}A_0 P_0^{\alpha-1} \\ \beta k_{PA}P_0 A_0^{\beta-1} & D_P k^2 + k_{\text{off},P} + \Psi k_{\text{on},P}\delta_{k,0} + k_{PA}A_0^{\beta} \end{pmatrix}. \tag{6}$$

An instability occurs if there exists at least one growth rate σ of $\tilde{J}$ with positive real part. Note that the global averages $\left\langle u_P \right\rangle$ and $\left\langle u_A \right\rangle$ give rise to the Kronecker-delta term $\delta_{k,0}$ which induces a discontinuously stabilizing shift of the zeroth Fourier mode $k_0 = 0$ (figure 1(B), α, β, red dot). As a consequence, and different from classical Turing diffusion driven instabilities, the mode that becomes unstable first and shows the fastest growth is given by $k_1 = 2\pi/L$. Thus, the pattern that is destabilized first and grows fastest always fits the system size. This will tend to divide the cell into two halves independent of size, which is an attractive property for cell polarity. Discontinuous growth rates are known from systems describing electro-chemical pattern formation as well as surface chemical reactions [13, 14] and are a consequence of

globally coupled systems. All the reaction–diffusion systems of type (4) show a discontinuous growth rate.

In studying the parameter dependence of this type of instability, we found a loop-shaped region in which at least one uniformly stable state becomes unstable with respect to nonuniform perturbations (figure 1(B), blue, blue dashed). Together, the regimes of uniform bistability, domains and linear instability form a characteristic topology (figure 1(C)) in which each distinctly colored region corresponds to a defined dynamic behavior of the system (see [6] for details). Interestingly, this parameter space topology is conserved even if other parameters such as the total protein concentrations $\rho_{0,P}$ and $\rho_{0,A}$ are varied while the interaction rate constants are kept fixed (figure 2(A)).

2.2. The wave-pinning model

The inhomogeneous domain states in the PAR protein model discussed above were found to be propagating fronts that stall based on the depletion of cytoplasmic protein supply [6]. This phenomenon has previously been highlighted in a simpler reaction–diffusion model and was termed wave-pinning [8]. In order to compare the two models, we now analyze the wave-pinning model in the same way as the PAR protein model.

Based on only one protein species ($N = 1$) that cycles between a cortical and a cytoplasmic compartment, the wave-pinning system conceptually describes polarization of small Rho-GTPases in the context of chemotaxis. Substituting the cytoplasmic variable $v(x, t)$ in the limit of infinitely fast cytoplasmic diffusion by $v(t) = \rho_0 - \langle u \rangle$, we reduce the originally proposed system of two differential equations to a single integro-differential equation of type (4). The kinetic function is then defined as:

$$f_1 = \left(\rho_0 - \langle u \rangle \right)\left(k_0 + \gamma \frac{u^2}{K^2 + u^2} \right) - \delta u, \tag{7}$$

where k_0 is the basal association rate, γ the maximal reaction rate above the base line, and K the saturation parameter. The linear stability analysis was computed analogously to the PAR protein model. With u_0 denoting the homogeneous steady-state, we find the growth rate of the wave-pinning model as

$$\sigma = -D_u k_f^2 + 2\gamma K^2 \frac{u_0 \left(\rho_0 - u_0 \right)}{\left(K^2 + u_0^2 \right)^2} - \delta - \left[k_0 + \gamma \frac{u_0^2}{K^2 + u_0^2} - \delta u_0 \right] \delta_{k_f,0}. \tag{8}$$

Note that the Fourier modes are denoted by k_f to avoid confusion with the reaction parameters k_0 and K. Similar to (6), $\delta_{k_f,0}$ symbolizes the Kronecker-delta while δ is a reaction parameter.

By applying the same analysis of uniform states, their stability properties and domain states to the wave-pinning model, we find a topology identical to the PAR protein model (figure 2(B)), despite differences in both the number of involved protein species and the kinetic function. The region of homogeneous bistability (figure 2(B), orange, compare to figure 1) again culminates in a cusp bifurcation. The region of linear instability loops around the cusp point, this time forming a distorted structure. Finally, the instability loop is enclosed by the comet-shaped region of inhomogeneous domain states which eventually crosses into the bistability regime, a property also observed in the PAR protein model for larger values of ρ_0's or $k_{AP/PA}$.

We used the parameters as reported in the published work [8], specifically $\gamma = 1\text{s}^{-1}$, $K = 1\,\mu\text{m}^{-1}$, $\delta = 1\text{s}^{-1}$ and $D_u = 0.1\mu\text{m}^2\text{s}^{-1}$. Simulations were carried out with $\Delta t = 0.0004$ s in a system of $L = 10\mu$m with 100 grid points spaced $\Delta x = 0.1\,\mu$m apart and no-flux boundary conditions.

The authors reported in their original work [8] that the model does not polarize spontaneously but requires a finite, possibly small stimulus in order to form patterns. The parameter space now shows that this threshold behavior is parameter specific. In particular, the chosen parameter set (figure 2(B), star) places the model close to but still outside the regime of linear instability where the single metastable uniform state is separated from the coexisting domain state by a threshold of variable size [6]. Slight displacement of parameters towards larger total protein concentration, would allow this system to polarize spontaneously. Thus, this topological analysis helps to reevaluate previously reported behaviors of the wave-pinning model.

2.3. The Rho-GTPase model

The wave-pinning model of the previous section highlighted principles that were underlying a more complex and biochemically accurate system for polarization of three small Rho-GTPases CDC-42 ($i \equiv C$), Rac ($i \equiv R$) and Rho ($i \equiv \rho$) in chemotaxis [2]. We therefore now analyze this third model. After reduction to three integro-differential equations in the limit of rapid cytoplasmic diffusion, the kinetic functions are defined as

$$
f_C = \frac{I_C}{1 + \left(u_\rho/\beta_\rho\right)^n} \frac{\rho_{0,C} - \langle u_C \rangle}{\rho_{0,C}} - \delta_C u_C
$$

$$
f_R = \left(I_R + \alpha_C u_C\right) \frac{\rho_{0,R} - \langle u_R \rangle}{\rho_{0,R}} - \delta_R u_R
$$

$$
f_\rho = \frac{I_\rho + \alpha_R u_R}{1 + \left(u_C/\beta_C\right)^n} \frac{\rho_{0,\rho} - \langle u_\rho \rangle}{\rho_{0,\rho}} - \delta_\rho u_\rho, \tag{9}
$$

wherein $I_{C/R/\rho}$, $\alpha_{C/R}$ and $\delta_{C/R/\rho}$ denote reaction rate constants, $\beta_{C/\rho}$ regulate Hill function dynamics and n is the Hill coefficient. The linear stability analysis was again computed analogously to the PAR protein model. We find the following form of the Jacobian in Fourier space:

$$
\tilde{J} =
-\begin{pmatrix}
-D_m k^2 - \delta_C - \lambda_C \delta_{k,0} & 0 & -4\dfrac{\rho_0^3}{\beta_\rho^4} \dfrac{I_C\left(C_{\text{tot}} - C_0\right)}{C_{\text{tot}}\left(1 + \left(\rho_0/\beta_\rho\right)^4\right)^2} \\[4mm]
\alpha_C \dfrac{R_{\text{tot}} - R_0}{R_{\text{tot}}} & -D_m k^2 - \delta_R - \lambda_R \delta_{k,0} & 0 \\[4mm]
-4\dfrac{C_0^3}{\beta_C^4} \dfrac{\left(I_\rho + \alpha_R R_0\right)\left(\rho_{\text{tot}} - \rho_0\right)}{\rho_{\text{tot}}\left(1 + \left(C_0/\beta_C\right)^4\right)^2} & \dfrac{\alpha_R\left(\rho_{\text{tot}} - \rho_0\right)}{\rho_{\text{tot}}\left(1 + \left(C_0/\beta_C\right)^4\right)} & -D_m k^2 - \delta_\rho - \lambda_\rho \delta_{k,0}
\end{pmatrix}. \tag{10}
$$

Here C_0, R_0 and ρ_0 denote the homogeneous steady-state. $\delta_{k,0}$ again symbolizes the Kronecker-delta which induces the discontinuous shift in the growth rates, and the prefactors are given by

$$\lambda_C = \frac{I_C}{C_{\text{tot}}\left(1 + \left(\rho_0/\beta_\rho\right)^4\right)}, \quad \lambda_R = \frac{I_R + \alpha_C C_0}{R_{\text{tot}}}, \quad \lambda_\rho = \frac{I_\rho + \alpha_R R_0}{\rho_{\text{tot}}\left(1 + \left(C_0/\beta_C\right)^4\right)}. \quad (11)$$

We used the parameters reported in the original publication [2], specifically $R_{\text{tot}} = 7.5\,\mu\text{M}$, $I_C = 3.4\,\mu\text{Ms}^{-1}$, $I_R = 0.5\,\mu\text{Ms}^{-1}$, $I_\rho = 3.3\,\mu\text{Ms}^{-1}$, $\alpha_C = 4.5\text{s}^{-1}$, $\alpha_R = 0.3\text{s}^{-1}$, $\beta_C = 1\,\mu\text{M}$, $\beta_\rho = 1.25\,\mu\text{M}$, $\delta_C = \delta_R = \delta_\rho = 1\text{s}^{-1}$, $D_{u,C} = D_{u,R} = D_{u,\rho} = 0.1\,\mu\text{m}^2\text{s}^{-1}$ and $n = 4$. Simulations were carried out with $\Delta t = 0.01\text{s}$ in a system of $L = 10\mu\text{m}$ with 100 grid points spaced $\Delta x = 0.1\mu\text{m}$ apart and no-flux boundary conditions.

Analyzing this system, we find the same parameter space topology as in the wave-pinning and PAR model, comprising a cusp bifurcation surrounded by an instability loop and enclosed in a comet-shaped region of nonuniform domains (figure 2(C)). Importantly, the common topology implies an identical repertoire of possible behaviors across all three models despite different numbers of protein species as well as different kinetic functions.

3. A minimal model for cell polarity

Motivated by the common parameter space topology, we next sought to construct a representative model that exhibits all topological features in a simple form, and also illustrates the reduction process. We now formulate such a minimal model of the type of (4) in which all topological features can be described analytically.

Only one protein species ($N = 1$) is necessary to exhibit the desired topology. Furthermore, bistability of homogeneous states with a cusp bifurcation appears as a hallmark property of the family of models discussed here. The simplest function that reproduces bistability with a cusp bifurcation is the well-studied cusp normal form [15]. This normal form can be derived locally around the cusp point of generic dynamical systems by a weakly nonlinear analysis [16, 17]. Here, we define the kinetic function of the minimal model such that elimination of the cytoplasmic variable by $v(t) = \rho_0 - \langle u \rangle$ leads to the cusp normal form extended by a global averaging term

$$\begin{aligned} f &= \eta v + \mu_1 u - u^3 \\ &= \eta\rho_0 - \eta\langle u \rangle + \mu_1 u - u^3. \end{aligned} \quad (12)$$

While the three previously discussed models produced positive concentrations, equation (12) exhibits negative values as well, thereby ruling out the interpretation of $u(x, t)$ as physical concentration. We use (12) as purely conceptual model that makes the parameter space accessible analytically, and similar arguments have been given elsewhere [8, 18].

3.1. Nondimensionalization

In the minimal model, one dynamical species ($N = 1$) is cycling between a state u with slow diffusion D_u and a state v subject to fast diffusion D_v. In the case of finite diffusion D_v the generic

formulation is given by

$$\frac{\partial \tilde{u}}{\partial \tilde{t}} = \tilde{D}_u \frac{\partial^2 \tilde{u}}{\partial \tilde{x}^2} + f\left(\tilde{u}, \tilde{v}\right), \quad f\left(\tilde{u}, \tilde{v}\right) = \tilde{\eta}\tilde{v} + \tilde{\mu}_1 \tilde{u} - \sigma\tilde{u}^3$$

$$\frac{\partial \tilde{v}}{\partial \tilde{t}} = \tilde{D}_v \frac{\partial^2 \tilde{v}}{\partial \tilde{x}^2} - f\left(\tilde{u}, \tilde{v}\right), \quad \tilde{\rho}_0 = \frac{1}{L}\int_0^L \tilde{u}(\tilde{x}, \tilde{t}) + \tilde{v}(\tilde{x}, \tilde{t})\,\mathrm{d}\tilde{x}.$$

Herein, the parameters have the dimensions $\left[\tilde{\eta}\right] = \left[\tilde{\mu}_1\right] = \mathrm{s}^{-1}$, $\left[\sigma\right] = \mathrm{m}^2\mathrm{s}^{-1}$ and $\left[\tilde{D}_u\right] = \left[\tilde{D}_v\right] = \mathrm{m}^2\mathrm{s}^{-1}$. We chose typical scales for length L and concentration U, from which we define a scale of time as $T = \left(\sigma\, U^2\right)^{-1}$ such that $\tilde{x} = Lx$, $\tilde{u} = Uu$ and $\tilde{t} = Tt$. Nondimensionalization then results in

$$\frac{\partial u}{\partial t} = D_u \frac{\partial^2 u}{\partial x^2} + f(u, v), \quad f(u, v) = \eta v + \mu_1 u - u^3$$

$$\frac{\partial v}{\partial t} = D_v \frac{\partial^2 v}{\partial x^2} - f(u, v), \quad \rho_0 = \int_0^1 u(x, t) + v(x, t)\,\mathrm{d}x, \tag{13}$$

where the nondimensional parameters are defined as $\eta = \tilde{\eta}\left(\sigma U^2\right)^{-1}$, $\mu_1 = \tilde{\mu}_1\left(\sigma U^2\right)^{-1}$, $D_u = \tilde{D}_u\left(L^2\sigma U^2\right)^{-1}$ and $D_v = \tilde{D}_v\left(L^2\,\sigma U^2\right)^{-1}$. Parameters were chosen as $\eta = 1$ and $D_u = 10^{-4}$. Simulations were run with $\Delta t = 0.01$ in a system of $L = 1$ with 400 grid points spaced $\Delta x = 0.0025$ apart and periodic boundary conditions.

3.2. Reduction process

Using the minimal model we here illustrate the implications that arise from the reduction from $2N$ differential equations with N conservation laws (equations (1)–(3)) to N integro-differential equations (in the form of (4)) in the limit of rapid cytoplasmic diffusion, a process that has been applied to all analyzed models.

The homogeneous system without diffusion can be illustrated in phase space of the two dynamic variables u_0 and v_0 (figure 3(A)). For a given set of parameters, the uniform steady-states of a mass-conserved system must satisfy $f\left(u_0, v_0\right) = 0$, which defines a curve in phase space (figure 3(A), dotted line). Its intersection with the lines $\rho_0^{1,2}$ for constant mass determines the uniform steady-state concentrations (figure 3(A), blue filled circle, see also [19]). Importantly, any perturbation of the uniform steady-state that respects conservation of mass (figure 3(A), green solid arrow) can only move the system to another point along the same line of mass (figure 3(A), blue open circle) from which it relaxes back to the same steady-state. Any motion perpendicular to that line (figure 3(A), green dashed arrow) corresponds to a change of mass, and hence is forbidden (figure 3(B)).

The homogeneous two-equation system can be exactly reduced to one-equation by substituting $v_0 = \rho_0 - u_0$, thereby incorporating the previously external constraint ρ_0 explicitly into the equations. As a consequence, the previously 2D phase space collapses to a 1D line along which any perturbation respects the conservation law (figure 3(C), green solid arrow).
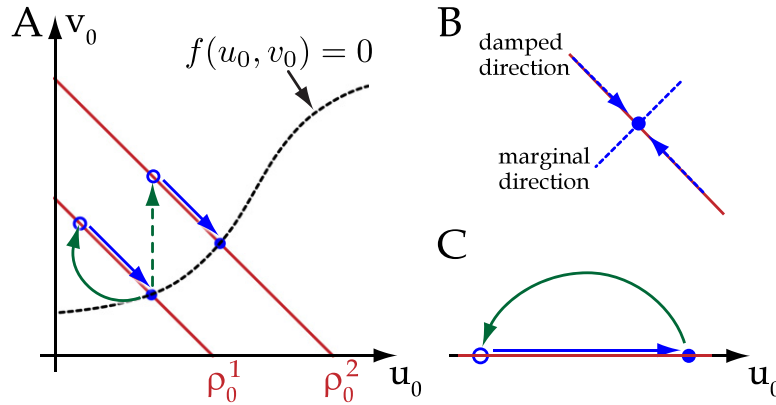
Figure 3. In the 2D phase space of the uniform system, movements are constrained by the conservation law. (A) Schematic of phase space. Red lines represent all states allowed for a system with conserved amount $\rho_0^{1,2}$. Blue solid circles represent the steady-states that are determined as intersection with the line $f\left(u_0, v_0\right) = 0$. A perturbation that respects conservation of mass (green solid arrow) leads to another point on the same line (blue open circle) from which the system relaxes back to the steady-state (blue arrow). A perturbation that violates mass conservation, e.g. by changing v_0 while leaving u_0 constant (green dashed arrow), leads to a system on a different line with ρ_0^2 from which the system relaxes to a new steady-state. (B) The dynamics of the system along the line of constant protein amount is damped with growth rate $\lambda_- = f_u - f_v$. However, the forbidden dynamic perpendicular to the lines is reflected in the marginal growth rate $\lambda_+ = 0$. (C) In the reduced system, the variable v_0 is replaced by $\rho_0 - v_0$. Since there is no restriction on the perturbations of the one-variable system, the marginal growth rate is eliminated and replaced by the damped value λ_-, hence leading to a discontinuously displaced zeroth Fourier mode.

3.3. Linear stability analysis of the minimal model

We begin the analytical description of the parameter space by highlighting the bistability region. For a homogeneous system, diffusion is absent and the global coupling simplifies to $\langle u \rangle = u$. Then, the region of bistability is known to be bounded by [20]

$$\rho_0 = \pm 2 \frac{\mu_1 - \eta}{3\eta} \sqrt{\frac{\mu_1 - \eta}{3}}, \tag{14}$$

with the cusp bifurcation occurring at $\mu_1 = \eta = 1$ (figure 5(A)).

Next, we turn to derive an analytical form of the instability loop. Linearizing equations (13) around the homogeneous steady-states $\left(u_0, v_0\right)$ leads to a Jacobian of the form

$$J = \begin{pmatrix} f_u - D_u k^2 & f_v \\ -f_u & -f_v - D_v k^2 \end{pmatrix}, \tag{15}$$
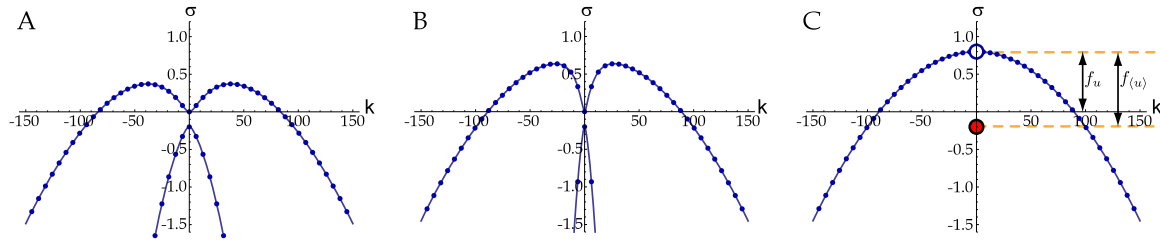
Figure 4. Rapid cytoplasmic diffusion leads to a discontinuously stabilized zeroth Fourier mode. Shown are the two growth rates $\sigma_{\pm}(k)$ for the two-variable minimal model with cytoplasmic diffusion $D_v = 10^{-3}$ (A) and $D_v = 10^{-2}$ (B) and the single growth rate σ for infinite cytoplasmic diffusion $D_v \to \infty$ in the reduced system (C) with $\mu_1 = 0.8, \eta = 1$ and $D_u = 10^{-4}$. Solid lines indicate continuous functions for an infinitely long system, blue dots represent discretization for a finite system length of $L = 1$. Red dot in C highlights the discontinuously shifted zeroth Fourier mode k_0.

with eigenvalues

$$\sigma_{\pm} = 1/2 \Big[\big(f_u - f_v - (D_v + D_u)k^2 \big)$$
$$\pm \sqrt{\big(f_u - f_v - (D_v + D_u)k^2 \big)^2 - 4 \big[D_u D_v k^4 + \big(D_u f_v - D_v f_u \big) k^2 \big]} \Big]. \quad (16)$$

For the uniform system $k = 0$, the smaller eigenvalue occurs at $\sigma_- = f_u - f_v$, while the larger eigenvalue is always marginal $\sigma_+ = 0$, such that the overall response of the system to any homogeneous perturbation will be a relaxation back to the uniform steady-state. The marginal growth rate at $k = 0$ enforces any band of unstable wave numbers to range from $0 \leqslant k \leqslant k_c$, an interval that is not strictly bounded away from $k = 0$. As a consequence, the emerging pattern will occur on a large length-scale close to the instability threshold. We identify this as type II long-wave instability as defined in [21].

For increased cytoplasmic diffusion, the magnitude of the growth rate of the membrane-bound variable increases and its maximum moves toward $k = 0$ (figures 4(A), (B)). For rapid cytoplasmic diffusion $D_v \to \infty$ and substitution of the cytoplasmic concentration by $v_0(t) = \rho_0 - 1/L \int u(x, t) \mathrm{d}x$, one of the growth rates is eliminated, leaving only its maximum as displaced node at $k = 0$ (figure 4(C)).

The single remaining growth rate is in general described by

$$\sigma = -D_u k^2 + f_u + f_{\langle u \rangle} \delta_{k,0}.$$

For the specific case of the kinetic function in (12) this reduces to

$$\sigma(k) = -D k^2 + \mu_1 - 3u_0^2 - \eta \, \delta_{k,0}. \quad (17)$$

The Kronecker-Delta symbol $\delta_{k,0}$ arises from Fourier transformation of the global coupling $\langle u \rangle$. The magnitude of the discontinuous shift $f_{\langle u \rangle}$ is given by $f_{\langle u \rangle} = \partial v / \partial \langle u \rangle \cdot \partial f / \partial v = -f_v$. Therefore, the new position of the homogeneous mode is the tip of the second growth rate $\sigma_-(k_0) = f_u - f_v$ that was eliminated in the reduction process (figure 4(B)). From the growth
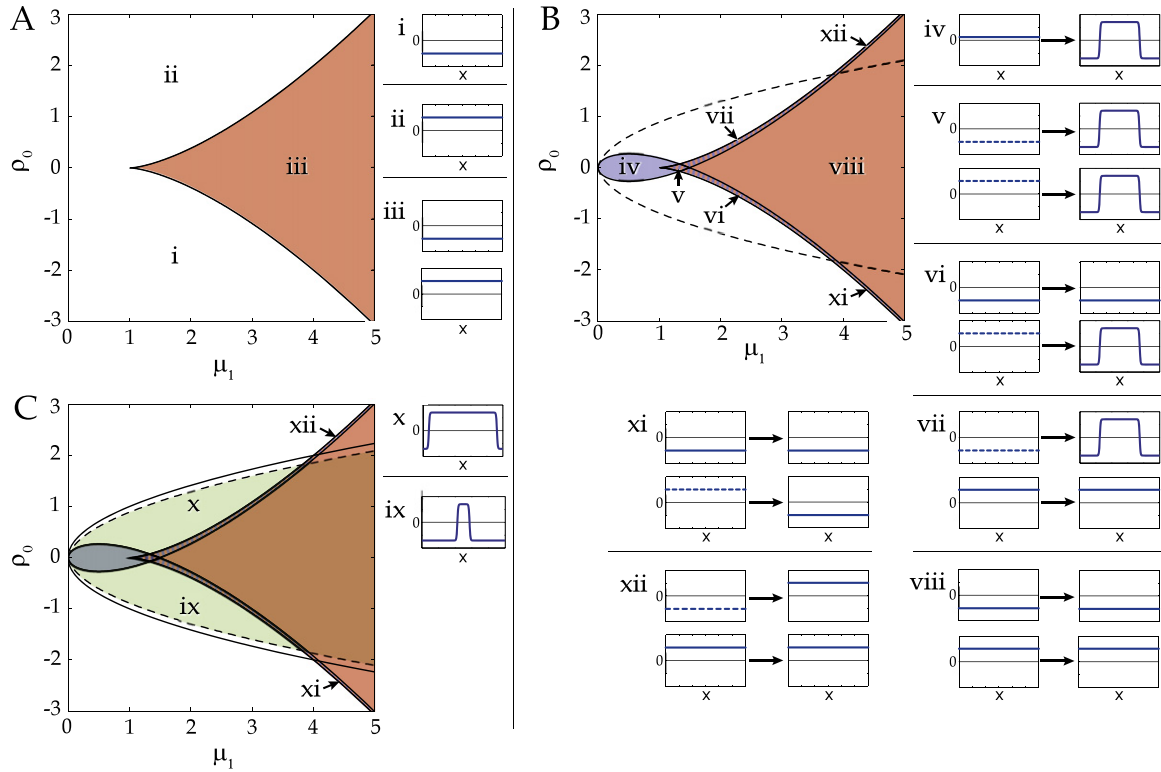
Figure 5. A minimal model makes the topology accessible analytically. Shown here are the region of bistability (A), linear instability (B) and existence of nonuniform domains (C) analogously to figure 1. Schematic concentration profiles show the uniform steady-states (A) (i)–(iii), their individual response to small spatially inhomogeneous perturbations (B) (iv)–(viii), (xi)–(xii), and the typical shape of domain profiles (C) (xi)–(x). Perturbations either decay for stable uniform states ((B), solid lines) or grow for unstable states ((B), dashed lines). The solid line that encloses the domain region in panel (C) is given by equation (19) and marks the maximum extend of the domain region for $D_u \to 0$, $D_u \neq 0$.

rate and the homogeneous steady-state we find the analytical form of the instability loop in parameter space as the function (figure 5(B), blue, blue dashed):

$$\rho_0 = \pm \frac{1}{\eta} \left(2\frac{\mu_1}{3} - \eta + \frac{1}{3}D_u k_1^2 \right) \sqrt{\frac{\mu_1 - D_u k_1^2}{3}}, \tag{18}$$

which has to be evaluated at the first unstable node $k_1 = 2\pi/L$. Thus, smaller system lengths L or larger diffusion constants D_u lead to shrinkage of the region of instability.

3.4. Inhomogeneous domain states

Finally, we investigate the inhomogeneous domain states of the minimal model. Numerical integration of equation (4) with the function f given in equation (12) shows that the nonuniform concentration profiles are front solutions, as before. Furthermore, they are found to exist in the familiar comet-shaped region (figure 5(C), green with dashed boundary) touching the instability loop at its tip. The simplicity of the minimal model allows to characterize this domain region

analytically [18]. Specifically, analytical calculation of the front propagation speed as a function of the uniform cytoplasmic concentration shows that the front reaches steady-state and stalls when $v = 0$, or equivalently $\langle u \rangle_0 = \rho_0$.

Using this stalling criterion and neglecting diffusion away from the front interfaces, we compute the domain width. From this, we find the lower and upper boundaries of the domain region in parameter space as the simple form

$$\rho_0 = \pm \sqrt{\mu_1}, \tag{19}$$

in good agreement with numerical simulations (see figure 5(C), solid line). Note that (19) can be rephrased as the necessary condition, $-\sqrt{\mu_1} < \rho_0 < \sqrt{\mu_1}$, on the protein amount that allows for front-stalling to occur.

3.5. The cusp bifurcation induces the instability loop

We noted earlier that the minimal model (12) represents a modified cusp normal form. Furthermore, we found that the bistability region with the cusp (14) and the instability loop (18) approach the same asymptotic function in the limit of large values of the parameter μ_1. Both observations raise the question if a cusp bifurcation is sufficient to give rise to the common topology of models described so far.

To investigate a possible connection between the cusp and instability loop in the minimal model, we focus on the growth rate (17) of the homogeneous system at $k_0 = 0$ (figure 6(B), top row) as a function of ρ_0 with different parameter values of μ_1 (figure 6(A)). As generic property of cusp bifurcations the single uniform state outside the bistability region is stable (figure 6(B), solid lines), while inside the bistability region two stable states (figure 6(B), blue and yellow) are separated by a third one (figure 6(B), red) that is unstable (figure 6(B), dashed lines). For the most unstable mode $k_1 \neq 0$ of the inhomogeneous system, we find that the growth rate is simply shifted upwards by a constant magnitude $\eta - D_u k_1^2$ everywhere in parameter space (figure 6(B), bottom row). This shift reveals that the uniformly stable states become unstable for spatial perturbations particularly close to the edges of the bistability region (figure 6(B), rightmost column), thereby causing the ascending and descending unstable branches along the boundary of the region of bistability (figure 6(A)). The shift in growth rates also explains that the cusp point always appears inside of the instability loop.

Because the shift between the growth rates of the uniform system $\sigma(k_0)$ and fastest growing mode of the nonuniform system $\sigma(k_1)$ is constant throughout parameter space, our minimal model relates the instability loop to the cusp bifurcation in a simple form. In more complex models, the shift will generally not be constant but parameter dependent. Consequently, the size of the unstable regions will also be dependent on their location in parameter space, hence leading to distortions and asymmetries of the loop as seen for instance in the wave-pinning model (7) (figure 2(B)).

Loop shaped regions of linear instabilities around a cusp bifurcation have been reported for other models unrelated to cell polarity. Examples include electrochemical systems where a diffusing species undergoes pattern formation due to the interaction with an electrical potential [22], as well as systems describing surface chemical reactions [14]. Furthermore, in absence of a Hopf bifurcation, the FitzHugh–Nagumo model shows classical Turing diffusion-driven
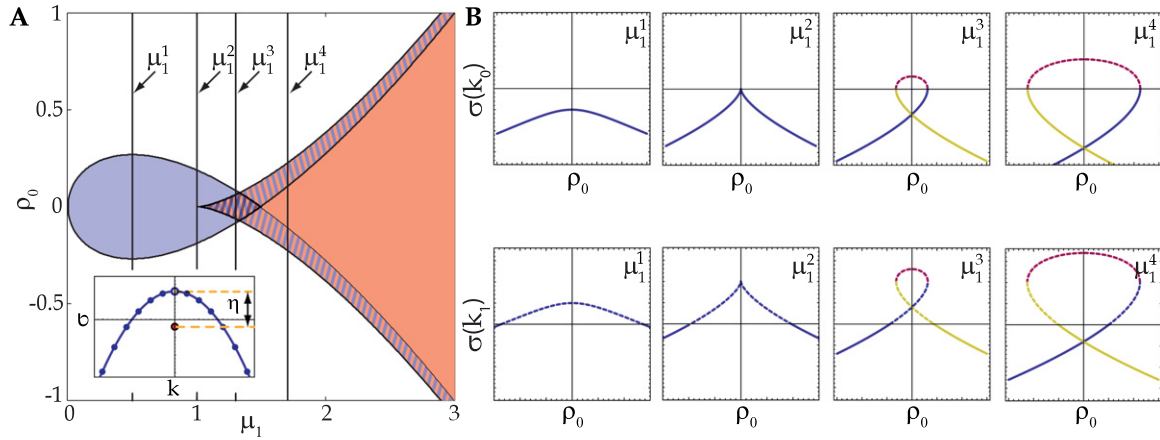
Figure 6. The instability structure of the cusp bifurcation induces the instability loop. (A) Region of bistability and instability in the minimal model (same color coding as in figure 5(B)). Inset schematically shows the structure of the growth rate. Vertical lines indicate cuts along ρ_0 for those four values of μ_1 that are investigated in panel (B). (B) Top row shows the growth rates for uniform perturbations $\sigma(k_0)$ as a function of ρ_0 for the four values of μ_1 indicated in panel (A). For $\mu_1^{1,2}$ only one stable uniform state exists (blue, solid lines). For $\mu_1^{3,4}$ inside the bistable region, two stable steady-states (blue, yellow, solid lines) are separated by a coexisting unstable state (red, dashed line). Bottom row shows the growth rate for the fastest growing mode $\sigma(k_1)$ which is identical to $\sigma(k_0)$ shifted upwards by an amount $\eta - D_u k_1^2$.

instabilities in the form of a loop around a cusp bifurcation [23]. Taken together, these examples suggest that the cusp bifurcation gives rise to the loop shaped region of linear instability.

We next ask the question if bistability of uniform states via a cusp bifurcation also implies inhomogeneous patterns that are front solutions and stall via a wave-pinning type mechanism. To answer this question, we consider a one-species ($N = 1$) conceptual model for CDC-42 polarization in yeast [4]. After the reduction for rapid cytoplasmic diffusion $v(t) = \rho_0 - \langle u \rangle$, the kinetic function of this model is given by

$$f = E_c \alpha u^2 \left(\rho_0 - \langle u \rangle \right) + E_c \beta u \left(\rho_0 - \langle u \rangle \right) - \gamma u + \epsilon, \tag{20}$$

wherein $E_c = E_c^0 \left(1 + \int_S g(u) \mathrm{d}s \right)^{-1}$ represents a conservation law for one of the parameters. As the authors note, this second integral constraint is not necessary for the pattern forming ability of equation (20) and we therefore ignore it here, setting $E_c \equiv 1$. An additional parameter ϵ was added to equation (20) which takes the value $\epsilon = 0$ in the original work.

This model shows bistability of homogeneous states with a cusp bifurcation under variations of parameters γ and ϵ. Moreover, a region of instability loops around the cusp point, albeit in strongly distorted form. However, the inhomogeneous patterns can not be propagating front solutions because this model violates the conditions necessary for wave-pinning to occur [8]. Thus, bistability via a cusp bifurcation is coupled to the loop shaped region of instability, but is not sufficient for front-like inhomogeneous patterns.

4. Discussion

Reaction–diffusion systems have been applied to a wide-range of contexts ranging from ecological to subcellular scales [24]. Instrumental for this is the freedom in the design of governing equations in terms of the number of involved protein species as well as the kinetic functions that define their interactions.

However, the complexity of spatially extended, nonlinear dynamical systems and the diversity of model designs entails a range of difficulties as well. First, the comprehensive characterization of the repertoire of possible behaviors under large variations of parameters rather than for a single parameter set poses a challenge in any individual reaction–diffusion model. Second, it remains a nontrivial task to compare two distinct models by explicitly stating which behavior is common to both and which behavior is specific to one of the models. Specifically, it is rather unlikely to find two models that are clearly distinct, yet can both be characterized in the same framework. Third, even if models according to these criteria could be identified, more fundamental understanding about the origin of their similarity for example in form of a minimal model would be required.

Here, we have presented a family of reaction–diffusion models that meet all three of the above benchmark criteria. First, we recapitulated the comprehensive analysis of a reaction–diffusion system for cell polarity of PAR proteins with respect to existence of uniform steady-states, linear instabilities and the existence of inhomogeneous domain states. Second, we applied the same analysis to two other models that share the properties of mass-conservation, rapid cytoplasmic diffusion as well as bistability of the reaction rates, but otherwise differ in the number of interacting chemical species and in the kinetic functions. We found that the topology of the PAR protein model more generally captures this family of systems. Different models have traditionally been compared by classifying the interacting species as either activator, substrate or inhibitor [25], by classifying the type of instabilities [21], or more recently by defining abstract design principles necessary for a specific stalling behavior of patterns [8]. Still, the topological analysis presented here provides a more specific characterization about the actual behavior observable in the model.

Third, based on the cusp bifurcation normal form, we presented a representative minimal model in which all parameter space elements can be calculated analytically. From this minimal model, we demonstrated that the instability loop appears as a generic property of the cusp bifurcation. In other contexts, the instability that loops around the cusp bifurcation can be a Hopf instability [14], a classical Turing instability [23] (where the unstable wave numbers are strictly bound away from zero), a long-wave instability (where the unstable wave-numbers are not bound away from zero), or a displaced-node instability that appears as a limit of Turing and long-wave instability for infinitely rapid cytoplasmic diffusion (17). Examples for instabilities looping around a cusp point have been found in excitable systems [23], in electro-chemical settings [22] and in models of surface catalysis [14].

Other reported models for cell polarity differ to various degrees from the family of models discussed here. The model by Otsuji [3], for instance, does not show bistability of uniform steady-states, thus illustrating that inhomogeneous patterns can occur independent of bistability of homogeneous states. The inhomogeneous patterns themselves are not front solutions. The CDC-42 model [4], in contrast, features bistability of uniform steady-states and shows the cusp bifurcation and the instability loop. However, similar to the model by Otsuji, the patterns in the CDC-42 model can not be front solutions, thereby clarifying that bistability of uniform states is

not sufficient for wave-pinning like behavior. Finally, the family of models discussed here adds front-like inhomogeneous patterns in a comet-shaped region to the bistability of uniform states and the loop shaped region of instability, hence suggesting that the condition for front-stalling patterns [8] likely is the strongest condition that defines the topology described here.

To conclude, this work illuminates the need to investigate the parameter space of models for cell polarization, to judge the robustness of model behavior to changes in parameters, to uncover generic topological features and to describe the full range of dynamical behaviors.

Acknowledgments

References

[1] Goldstein B and Macara I G 2007 The PAR proteins: fundamental players in animal cell polarization *Dev. Cell* **13** 609–22

[2] Jilkine A, Marée A F and Edelstein-Keshet L 2007 Mathematical model for spatial segregation of the Rho-family GTPases based on inhibitory crosstalk *Bull. Math. Biol.* **69** 1943–78

[3] Otsuji M, Ishihara S, Co C, Kaibuchi K, Mochizuki A and Kuroda S 2007 A mass conserved reaction-diffusion system aptures properties of cell polarity *PLoS Comput. Biol.* **3** e108

[4] Goryachev A B and Pokhilko A V 2008 Dynamics of Cdc42 network embodies a Turing-type mechanism of yeast cell polarity *FEBS Lett.* **582** 1437–43

[5] Dawes A T and Munro E M 2011 PAR-3 Oligomerization may provide an actin-independent mechanism to maintain distinct par protein domains in the early caenorhabditis elegans embryo *Biophys. J.* **101** 1412–22

[6] Goehring N W, Khuc Trong P, Bois J S, Chowdhury D, Nicola E M, Hyman A A and Grill S W 2011 Polarization of PAR proteins by advective triggering of a pattern-forming system *Science* **334** 1137–41

[7] Otsuji M, Terashima Y, Ishihara S, Kuroda S and Matsushima K 2010 A conceptual molecular network for chemotactic behaviors characterized by feedback of molecules cycling between the membrane and the cytosol *Sci. Signal.* **3** ra89

[8] Mori Y, Jilkine A and Edelstein-Keshet L 2008 Wave-pinning and cell polarity from a bistable reaction–diffusion system *Biophys. J.* **94** 3684–97

[9] Jilkine A and Edelstein-Keshet L 2011 A comparison of mathematical models for polarization of single eukaryotic cells in response to guided cues *PLoS Comput. Biol.* **7** 001121

[10] Govaerts W, Kuznetsov Y A, De Feo O, Dhooge A, Govorukhin V, Khoshsiar Ghaziani R, Meijer H G E, Mestrom W, Riet A and Sautois B 2008 MatCont continuation software in Matlab, version 2.5.1. *Technical Report* Universiteit Gent, Utrecht University (http://sourceforge.net/projects/matcont/ and http://www.matcont.UGent.be/)

[11] Wolfram Research 2008 Mathematica, Version 7.0 Wolfram Research (Champaign, Il)

[12] Howard J, Grill S W and Bois J S 2011 Turing's next steps: the mechanochemical basis of morphogenesis *Nat. Rev. Mol. Cell Biol.* **12** 392–8

[13] Krischer K, Mazouz N and Flätgen G 2000 Pattern formation in globally coupled electrochemical systems with an S-shaped current-potential curve *J. Phys. Chem.* B **104** 7545–53

[14] Hildebrand M 2002 Self-organized nanostructures in surface chemical reactions: mechanisms and mesoscopic modeling *Chaos* **12** 144–56

[15] Kuznetsov Y A 1998 *Elements of Applied Bifurcation Theory* (*Applied Mathematical Sciences*) 2nd edn (Berlin: Springer)

[16] Pismen L M 2006 *Patterns and Interfaces in Dissipative Dynamics* (Berlin: Springer)

[17] Rubinstein B, Slaughter B D and Li R 2012 Weakly nonlinear analysis of symmetry breaking in cell polarity models *Phys. Biol.* **9** 045006

[18] Mori Y, Jilkine A and Edelstein-Keshet L 2011 Asymptotic and bifurcation analysis of wave-pinning in a reaction–diffusion model for cell polarization *SIAM J. Appl. Math.* **71** 1401–27

[19] Ishihara S and Kaneko K 2006 Turing pattern with proportion preservation *J. Theor. Biol.* **238** 683–93

[20] Strogatz S H 2001 *Nonlinear Dynamics and Chaos: With Applications to Physics, Biology, Chemistry and Engineering* (Cambridge, MA: Perseus Books Group)

[21] Cross M C and Hohenberg P C 1993 Pattern formation outside of equilibrium *Rev. Mod. Phys.* **65** 851

[22] Mazouz N and Krischer K 2000 A Theoretical study on turing patterns in electrochemical systems *J. Phys. Chem.* B **104** 6081–90

[23] Metens S, Dewel G, Borckmans P and Engelhardt R 1997 Pattern selection in bistable systems *Europhys. Lett.* **37** 109–14

[24] Murray J D Jan 2003 *Mathematical Biology II* (Berlin: Springer)

[25] Gierer A and Meinhardt H 1972 A theory of biological pattern formation *Kybernetik* **12** 30–39